ACS Chemical Neuroscience

Research Article

pubs.acs.org/chemneuro

Stapled Voltage-Gated Calcium Channel (Ca_V) α-Interaction Domain (AID) Peptides Act As Selective Protein−Protein Interaction Inhibitors of Ca_V Function

Felix Findeisen,[†] Marta Campiglio,[‡] Hyunil Jo,[†,§] Fayal Abderemane-Ali,[†] Christine H. Rumpf,[†] Lianne Pope,[†] Nathan D. Rossen,[†] Bernhard E. Flucher,[‡] William F. DeGrado,[†,§] and Daniel L. Minor, Jr.*[,†,∥,⊥,▽,○]

[†]Cardiovascular Research Institute and [‡]Division of Physiology, Department of Physiology and Medical Physics, Medical University Innsbruck, 6020 Innsbruck, Austria

[§]Departments of Biochemistry and Biophysics, and Cellular and Molecular Pharmacology, [∥]Department of Pharmaceutical Chemistry, [⊥]California Institute for Quantitative Biomedical Research, and [▽]Kavli Institute for Fundamental Neuroscience, University of California, San Francisco, California 93858-2330, United States

[○]Molecular Biophysics & Integrated Imaging Division, Lawrence Berkeley National Laboratory, Berkeley, California 94720, United States

Supporting Information

ABSTRACT: For many voltage-gated ion channels (VGICs), creation of a properly functioning ion channel requires the formation of specific protein−protein interactions between the transmembrane pore-forming subunits and cytoplasmic accessory subunits. Despite the importance of such protein−protein interactions in VGIC function and assembly, their potential as sites for VGIC modulator development has been largely overlooked. Here, we develop *meta*-xylyl (*m*-xylyl) stapled peptides that target a prototypic VGIC high affinity protein−protein interaction, the interaction between the voltage-gated calcium channel (Ca_V) pore-forming subunit α-interaction domain (AID) and cytoplasmic β-subunit ($Ca_V\beta$). We show using circular dichroism spectroscopy, X-ray crystallography, and isothermal titration calorimetry that the *m*-xylyl staples enhance AID helix formation are structurally compatible with native-like AID:$Ca_V\beta$ interactions and reduce the entropic penalty associated with AID binding to $Ca_V\beta$. Importantly, electrophysiological studies reveal that stapled AID peptides act as effective inhibitors of the $Ca_V\alpha_1$:$Ca_V\beta$ interaction that modulate Ca_V function in an $Ca_V\beta$ isoform-selective manner. Together, our studies provide a proof-of-concept demonstration of the use of protein−protein interaction inhibitors to control VGIC function and point to strategies for improved AID-based Ca_V modulator design.

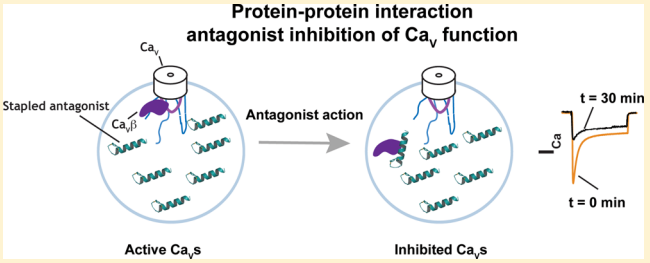

KEYWORDS: *Voltage-gated calcium channel (Ca_V), AID:$Ca_V\beta$ interaction, stapled peptide, protein−protein interaction antagonist, X-ray crystallography, electrophysiology*

INTRODUCTION

Voltage-gated ion channels (VGICs) control electrical signaling in the brain, heart, and nervous system.[1] Many members of this protein superfamily are multiprotein complexes comprising both transmembrane pore-forming subunits and cytoplasmic regulatory subunits.[2] VGIC cytoplasmic subunits can exert strong control over channel function by conferring distinct biophysical properties to the resulting channel complex and by affecting channel biogenesis and plasma membrane trafficking.[1,3−5] Although the importance of such subunits for VGIC function is well established, with the exception of a few cases,[6−9] their potential as targets for the development of agents that could control channel function has been largely overlooked.[10−12] Protein−protein interaction antagonists have been shown to be effective modulators of diverse protein classes[13−17] but have not yet been developed and validated for any ion channel system. Hence, we asked whether we could advance this type of reagent against the exemplar VGIC high-affinity protein−protein interaction formed between the voltage-gated calcium channel pore-forming $Ca_V\alpha_1$ and cytoplasmic $Ca_V\beta$ subunits for which there is a wealth of structural information to guide design.[18]

High-voltage Ca_Vs (Ca_V1s and Ca_V2s) are the principal agents of calcium influx in excitable cells, are vital components of the machinery that regulates muscle contraction, vascular tone, hormone and neurotransmitter release, and synaptic

Received: December 23, 2016
Accepted: March 9, 2017
Published: March 9, 2017

DOI: 10.1021/acschemneuro.6b00454
ACS Chem. Neurosci. 2017, 8, 1313−1326

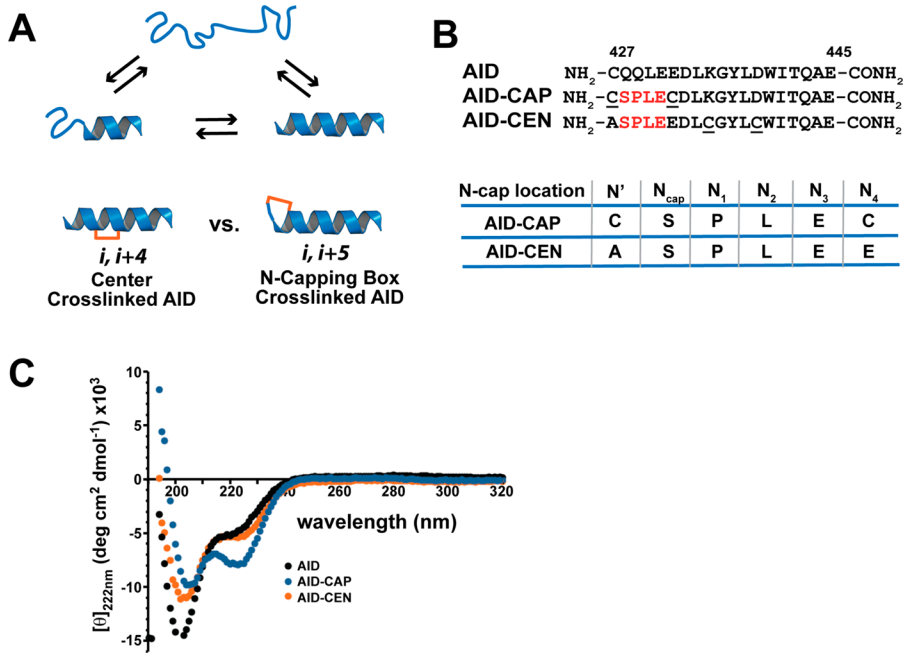

Figure 1. Backbone staples increase AID helical content. (A) Schematic showing the conformational ensemble of the native AID (top) versus the desired effect of incorporating the *m*-xylyl backbone staple. (B) AID, AID-CAP, and AID-CEN peptide sequences. The capping box residues are highlighted in red. Underline denotes *m*-xylyl linker cross-linking positions. (C) Circular dichroism spectra of AID (black), AID-CAP (blue), and AID-CEN (orange) at 70 μM and 4 °C.

function, and provide a prototypical example of the pivotal role of cytoplasmic subunits in VGIC function.[1,19−21] Ca_V1s and Ca_V2s are made from at least four main components:[18,22,23] a $Ca_V\alpha_1$ pore forming subunit, a cytoplasmic $Ca_V\beta$ subunit,[20,21] the extracellular $Ca_V\alpha_2\delta$ subunit,[24] and a calcium sensor protein, such as calmodulin.[25] The $Ca_V\alpha_1$:$Ca_V\beta$ interaction is central to the formation of properly functioning native Ca_Vs,[20,21] controls Ca_V trafficking to the plasma membrane,[3,26−30] and affects a number of Ca_V biophysical properties including voltage-dependent activation and the rate of channel inactivation.[20,21,31−39] $Ca_V\alpha_1$ and $Ca_V\beta$ associate through a high affinity (K_d approximately nanomolar)[40−45] interaction between a short peptide segment on the Ca_V intracellular I−II loop, known as the α-interaction domain (AID), and a groove in $Ca_V\beta$ termed the α-binding pocket (ABP).[20,46−49]

Ca_Vs are validated targets for drugs treating cardiovascular diseases, epilepsy, and chronic pain.[19,50] Well-studied modifiers of Ca_V function such as small molecule drugs and peptide toxins largely target the pore-forming subunit.[19,50−52] Because of the central role of the AID:ABP protein−protein interaction in Ca_V function, there has been an interest in establishing whether interfering with this interaction might provide an alternative strategy for Ca_V modulation.[45,53] Previous studies suggesting that the $Ca_V\alpha_1$:$Ca_V\beta$ interaction is labile[54−57] and studies showing that blocking $Ca_V\beta$ action is a productive means to affect Ca_V function[8,9] support such an approach.

Because, stapled-peptide strategies have been particularly effective at targeting protein−protein interactions in which one partner is single α-helix,[17,58] such as in the AID:ABP case, we pursued the stapled-peptide strategy to develop AID-based inhibitors of the AID:ABP interaction and Ca_V function. Previously, we and others demonstrated that chemical cross-linking of *i* and *i* + 4 cysteines could be useful for α-helical peptide stabilization.[59,60] Here, we expand this cysteine cross-linking strategy to constrain an N-terminal capping motif[61,62] appended to the AID. Our studies demonstrate that stapling AID peptides with a *meta*-xylyl bridge[59,63] between two engineered cysteines creates AID peptides having enhanced helical content that bind $Ca_V\beta$ in a native-like manner. We find that the macrocyclic constrained cap acts as an effective means to enhance helix content and that, importantly, the enhanced AID peptide is a potent inhibitor of Ca_V currents that causes $Ca_V\beta$ isoform-specific inhibition of the AID:ABP interaction.

RESULTS

AID Backbone Modifications Increase α-Helical Content of AID. Structural studies have shown that there is essentially no conformational change between the apo- and AID-bound $Ca_V\beta$ ABP.[46−48] By contrast, the Ca_V AID peptide undergoes a large conformational change between an unbound disordered state and the $Ca_V\beta$-bound helical conformation.[45,47,64,65] This binding event involves a substantial entropic penalty, approximately −14 cal mol^{-1} K^{-1},[45] that due to the essentially unchanged structure of the ABP must arise from the entropic cost of ordering the AID. In order to overcome this problem, we pursued a chemical stabilization strategy to enhance the helical structure of the AID unbound state (Figure 1A).

Previously, we and others demonstrated that introduction of *m*-xylyl linker between two cysteines (*i*, *i* + 4) by thiol alkylation[63] could be used to stabilize the α-helical conformation in peptides.[59,60] This cysteine alkylation strategy has the advantage of not requiring unnatural amino acids. To date, all strategies for stapled peptide synthesis have focused on introduction of linkers along one α-helix face, an approach that can buttress the structure but that does not restrain the α-helix polar ends. To address this issue, we introduced an N-terminal capping motif[61,62] into two AID peptides, AID-CAP and AID-CEN (Figure 1B). This capping motif includes an N_{Cap} position serine intended to stabilize the structure through hydrogen

DOI: 10.1021/acschemneuro.6b00454
ACS Chem. Neurosci. 2017, 8, 1313−1326

bonds to the exposed amide protons at the helix N-terminus, an N_1 position proline to act as a helix initiator, and an N_3 position glutamate placed to contribute hydrogen bonds to the N_{Cap} serine and amide backbone (Figure 1B). In the case of AID-CAP, two cysteines were included to make a macrocyclic capping box sequence, Cys-Ser-Pro-Leu-Glu-Cys, in which the cysteine residues should allow facile macrocyclization with *m*-xylyl bromide (Figure 1B). AID-CEN bears an unconstrained capping motif and a more conventional (i, i + 4) cross-linking motif within the helix (K435C and D439C) (Figure 1B). In both peptides, cysteine positions for staple attachment were chosen to reside on the exposed AID surface based on structures of the $Ca_V\beta$–AID complexes in order to avoid introducing interfering interactions.

Circular dichroism (CD) studies of AID-CAP and AID-CEN indicated that *m*-xylyl staple incorporation affected the secondary structure to different extents depending on the staple location (Figure 1C). The *m*-xylyl staple in AID-CEN caused a modest change that reduced the intensity of the signal at 208 nm relative to the unmodified AID. By contrast, AID-CAP displayed the hallmark double minima associated with α-helical structure that was absent in the unmodified AID peptide[66] and that indicates that the N-terminal cap site is a potent element for stabilizing the AID helical conformation.

X-ray Crystal Structures Show That $Ca_V\beta_{2a}$:Stapled AID Complexes Are Similar to Native Complexes. To investigate the structural integrity of the backbone staple designs, we crystallized and determined the structure of AID-CAP and AID-CEN bound to a unimolecular $Ca_V\beta_{2a}$ construct previously used for extensive $Ca_V\beta_{2a}$:AID thermodynamic binding studies.[45] Crystals of the AID-CAP complex grew in the *H*3 space group having one molecule in the asymmetric unit and diffracted X-rays to 1.9 Å (Table S1). Structure solution by molecular replacement (R/R_{free}= 18.5/23.0%) revealed a $Ca_V\beta_{2a}$:AID structure similar to that determined previously for the unconstrained AID[48] ($RMSD_{C\alpha}$ = 1.2 Å) (Figure 2A) except for a few minor differences. The $Ca_V\beta_{2a}$ α1 helix is longer by ten residues (Figure S1A), and there is a moderate divergence in the angle of the α2 helix. This element precedes the disordered V2/HOOK domain and extends from the SH3 domain far from the AID binding site (Figure S1A) and is affected by crystal lattice contacts. Excluding the α2 helix from the comparison, the structures of the $Ca_V\beta_{2a}$:AID- and $Ca_V\beta_{2a}$:AID-CAP complexes are essentially identical ($RMSD_{C\alpha}$= 0.55 Å over residues 43–127, 217–273, 295–414).

The structure of the $Ca_V\beta_{2a}$:AID-CAP complex (Figure 2A) reveals that the AID-CAP peptide binds to the α-binding pocket (ABP) in a manner that is identical to the wild-type AID (Figure S1A) using the main hydrophobic anchors Tyr437, Trp440, and Ile441 and interactions with two buried water molecules coordinated by the side chain of Ty437 (Figure S1B).[45−48] The *m*-xylyl linker connecting the $i \rightarrow i + 5$ cysteines was clearly visible in the electron density (Figure 2B). This moiety makes no interactions with $Ca_V\beta$, indicating that its effects are only on the AID conformational properties as intended. The N-terminal AID-CAP residue, Cys427, adopts a nonhelical conformation that occupies the β-backbone conformation portion of the Ramachandran plot. Subsequent residues form a regular α-helix. Within the *m*-xylyl stabilized region, the Glu431 side chain contacts the backbone nitrogen of Ser428, satisfying the backbone requirement for this otherwise free functional group and the intention of the sequence design. The cysteine members of the *m*-xylyl staple,

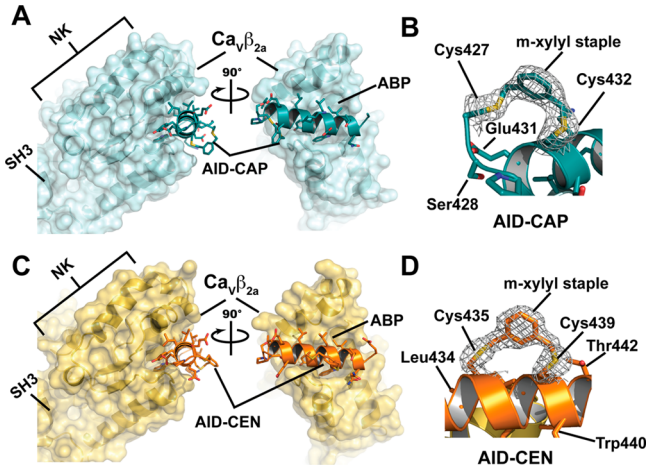

Figure 2. Crystal structures of $Ca_V\beta_{2a}$:stapled peptide complexes. (A) Structure of the $Ca_V\beta_{2a}$:AID-CAP complex. $Ca_V\beta_{2a}$ (cyan) is shown in surface rendering. AID-CAP (deep teal) is shown as a cartoon having side chains shown as sticks. Locations of the AID-CAP and ABP, nucleotide kinase (NK) and SH3 domains of $Ca_V\beta_{2a}$ are indicated. (B) $2F_o - F_c$ electron density (1.0σ) for the AID-CAP *m*-xylyl staple. Select AID-CAP residues are indicated. (C) Structure of the $Ca_V\beta_{2a}$:AID-CEN complex. $Ca_V\beta_{2a}$ (yellow orange) is shown in surface rendering. AID-CEN (orange) is shown as a cartoon having side chains shown as sticks. Locations of the AID-CEN and ABP, nucleotide kinase (NK), and SH3 domains of $Ca_V\beta_{2a}$ are indicated. (D) $2F_o - F_c$ electron density (1.0σ) for the AID-CEN *m*-xylyl staple. Select AID-CAP residues are indicated.

Cys427 and Cys432, have side chain χ1 angles of (+60°) and *meta* (−180°), respectively, resulting in a 5.9 Å distance between the Cys427 and Cys432 sulfurs that allows for unstrained connection through the *meta*-xylene functional group.

We also obtained crystals of the $Ca_V\beta_{2a}$:AID-CEN complex that grew in the $P2_12_12_1$ spacegroup, diffracted X-rays to 1.8 Å, and the structure was solved by molecular replacement (R/R_{free} = 15.8/19.6%) (Figure 2C, Table S1). In this structure, $Ca_V\beta_{2a}$ has an extended C-tail (residues 417–425) (Figure S1A), but otherwise, the $Ca_V\beta_{2a}$ component is essentially unchanged from the $Ca_V\beta_{2a}$ core[48] ($RMSD_{C\alpha}$ = 0.4 Å over residues 43–127, 217–273, 295–414) or $Ca_V\beta_{2a}$ in the $Ca_V\beta_{2a}$:AID-CAP complex (Figure 2C, $RMSD_{C\alpha}$ = 0.4 Å over residues 43–127, 217–273, 295–414). As with the $Ca_V\beta_{2a}$:AID-CAP complex, the AID-CEN backbone forms a regular α-helix and the $Ca_V\beta_{2a}$:AID-CEN interaction is unaltered from the native structure (Figure S1B). Density for the $i \rightarrow i + 4$ *m*-xylyl backbone staple was well resolved (Figure 2D) and shows that, similar to the situation with AID-CAP, the *m*-xylyl staple plays no direct role in in $Ca_V\beta$ binding. The cysteine anchors for the *m*-xylyl staple, Cys435 and Cys439, have side chain χ1 angles of −180° and −161°, respectively. This conformation leads to a 6.5 Å distance between the Cys435 and Cys439 sulfurs. The ∼20° deviation from the regular low energy conformers of Cys439 suggests that there is a small energetic cost for liganding the anchor atoms at a 6.5 Å distance. Comparison of the N-terminal capping motifs in the $Ca_V\beta_{2a}$:AID-CAP and $Ca_V\beta_{2a}$:AID-CEN complexes shows that the designed hydrogen bond network among the N_{Cap}, N_2, N_3, and N_4 positions is well formed in the presence of the AID-CAP *m*-xylyl staple (Figure S1C). This network is also present in the unconstrained capping motif in AID-CEN but has longer hydrogen bonds and

DOI: 10.1021/acschemneuro.6b00454
ACS Chem. Neurosci. 2017, 8, 1313−1326

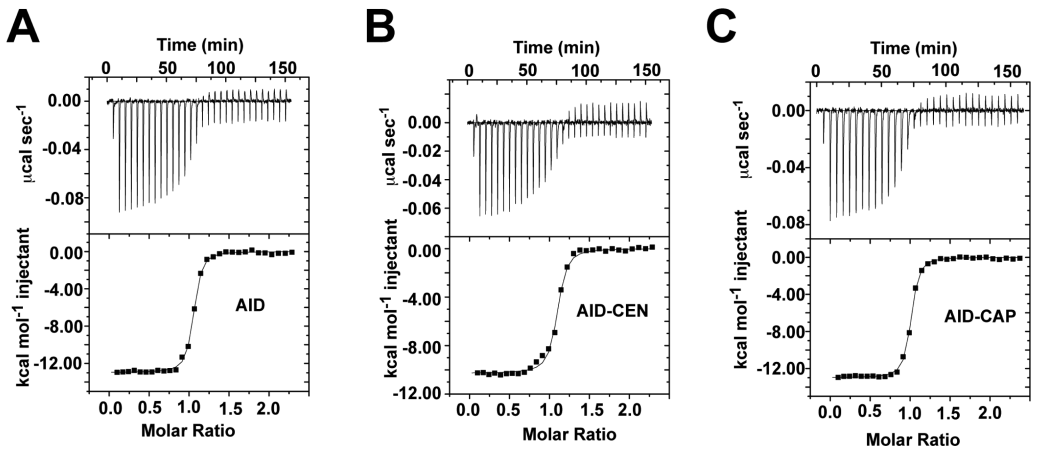

Figure 3. Backbone modifications decrease entropic cost of $Ca_V\beta_{2a}$ binding. Exemplar ITC titrations for (A) 20 μM AID into 2 μM $Ca_V\beta_{2a}$, (B) 20 μM AID-CEN into 2 μM $Ca_V\beta_{2a}$ core, and (C) 20 μM AID-CAP-peptide into 2 μM $Ca_V\beta_{2a}$.

Table 1. AID Peptide:$Ca_V\beta_{2a}$ Thermodynamic Binding Parameters

AID peptide	n	K_d (nM)	N	ΔH (kcal mol^{-1})	ΔS (cal mol^{-1} K^{-1})	K_d/K_d $Ca_V1.2$ AID
Cav1.2 AID	3	6.6 ± 2.0	0.94 ± 0.07	−15.6 ± 2.4	−16.7 ± 6.0	1
AID-CEN	2	5.2 ± 1.5	1.05 ± 0.03	−10.2 ± 0.1	2.2 ± 0.5	0.79 ± 0.33
AID-CAP	3	5.1 ± 1.6	1.02 ± 0.10	−12.3 ± 1.4	−4.6 ± 4.1	0.77 ± 0.34

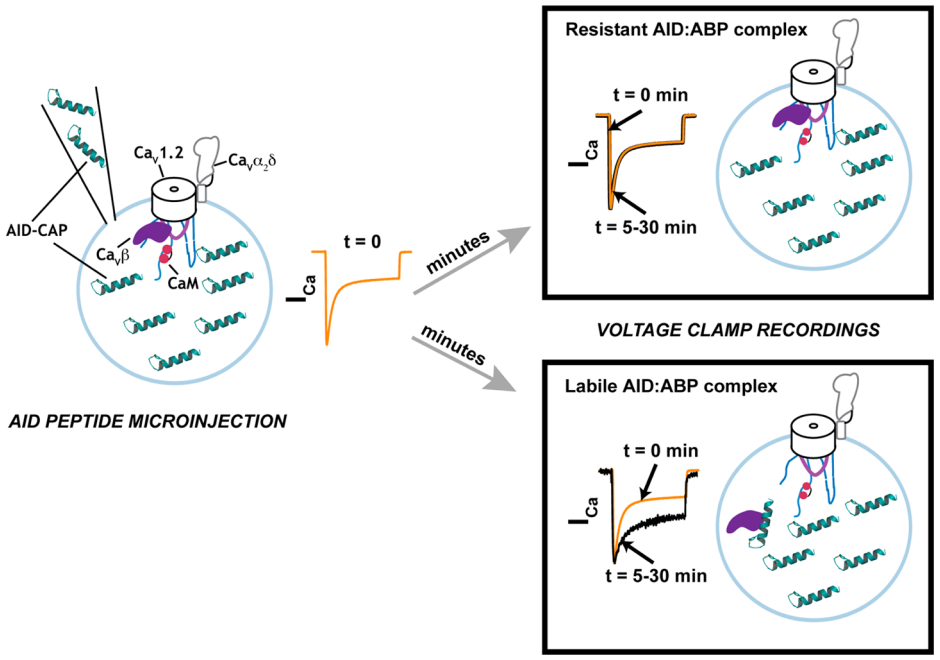

Figure 4. Schematic of AID peptide competition experiment. *Xenopus* oocytes expressing Ca_V channels (complexes of $Ca_V1.2$ (black lines), $Ca_V\beta$ (purple), $Ca_V\alpha_2\delta$ (gray lines), and CaM (red) (left) are injected with AID-CAP peptide at t = 0 and initial channel properties are recorded using two-electrode voltage clamp). Panels show two possible outcomes. Resistant complexes have no changes in channel biophysical properties (orange vs black lines). Labile channel complexes in which the AID competitor peptide can capture released $Ca_V\beta$ leaving an unoccupied I−II loop (purple) show biophysical changes. For simplicity, changes in channel current amplitude, an additional possible outcome for labile complexes, is not depicted.

slightly different interactions for Glu431 (Figure S1D). Together, the structural data demonstrate that the *m*-xylyl staple is compatible with the helical conformation of the AID and in the case of AID-CAP helps to organize the N-terminal capping motif.

AID Helix Staples Lower the Entropic Cost of Ligand Binding. Having determined that the backbone staples are able to affect AID helix content (Figure 1) and are structurally compatible with the $Ca_V\beta$-AID interaction (Figure 2), we used isothermal titration calorimetry (ITC) to investigate whether the AID staples impacted binding thermodynamics. Experiments measuring $Ca_V1.2$ AID binding to the $Ca_V\beta_{2a}$ core yielded an affinity in good agreement with prior measurements K_d = 6.6 ± 2.0 nM vs 5.3 nM[45] (Figure 3A, Table 1). This binding reaction is driven by a favorable enthalpic component (ΔH = −15.6 ± 2.4 kcal mol^{-1}) that is opposed by a large entropic cost (ΔS = −16.7 ± 6.0 cal mol^{-1} K^{-1}) that most

DOI: 10.1021/acschemneuro.6b00454
ACS Chem. Neurosci. 2017, 8, 1313−1326

Table 2. $Ca_V1.2$ Inactivation Parameters and GV Relationship[a]

		t_{i300} (%)	A_1 (%)	τ_1 (ms)	A_2 (%)	τ_2 (ms)	I_{max}	$V_{1/2}$	N
	$Ca_V1.2$:$Ca_V\beta_{2a}$	68.4 ± 1.1	49.4 ± 1.9	25.4 ± 1.2	21.3 ± 1.2	159.6 ± 8.4	−0.411 ± 0.054	8.1 ± 1.2	25
	$Ca_V1.2$-Y437A:$Ca_V\beta_{2a}$	66.0 ± 3.2	51.6 ± 3.7	31.2 ± 4.6	22.5 ± 3.9	177.3 ± 10.9	−0.816 ± 0.237	7.5 ± 1.4	6
	$Ca_V1.2$:$Ca_V\beta_3$	75.9 ± 1.1	70.3 ± 0.9	59.8 ± 2.5			−0.964 ± 0.008	5.5 ± 1.4	20
			59.9 ± 1.9	*33.9 ± 3.0*	*25.4 ± 1.6*	*312.0 ± 47.7*			
	$Ca_V1.2$, no $Ca_V\beta$	47.9 ± 1.2	26.8 ± 3.6	75.5 ± 10.3	48.4 ± 4.8	348.3 ± 41.4	−0.245 ± 0.028	18.1 ± 1.0	14
$Ca_V1.2$-Y437A:$Ca_V\beta_{2a}$	water 5 min	67.2 ± 1.9	51.9 ± 2.2	28.0 ± 1.5	19.7 ± 1.2	170.5 ± 6.3	−0.722 ± 0.092	7.8 ± 1.3	5
	water 30 min	59.8 ± 2.6	42.6 ± 2.6	31.6 ± 2.9	23.7 ± 1.6	200.5 ± 13.8	−0.430 ± 0.075	11.1 ± 1.2	5
	HotA, 5 min	68.8 ± 1.0	54.0 ± 1.2	33.2 ± 1.4	20.0 ± 1.3	212.5 ± 16.4	−1.001 ± 0.153	4.7 ± 1.4	18
	HotA, 30 min	63.7 ± 1.3	47.2 ± 1.2	34.5 ± 1.7	22.0 ± 1.0	197.9 ± 10.1	−0.578 ± 0.064	7.1 ± 1.1	18
	AID-CAP, 5 min	65.5 ± 1.3	52.7 ± 1.3	32.9 ± 1.7	18.8 ± 1.1	212.6 ± 18.6	−1.016 ± 0.122	5.4 ± 1.4	16
	AID-CAP, 30 min	43.1 ± 3.7	24.8 ± 3.2	52.8 ± 8.2	38.2 ± 3.0	469.8 ± 160.1	−0.156 ± 0.022	16.9 ± 1.0	15
	AID, 5 min	64.9 ± 1.9	48.5 ± 1.8	35.0 ± 1.5	24.1 ± 1.6	251.5 ± 16.1	−0.883 ± 0.111	2.9 ± 1.7	10
	AID, 30 min	44.8 ± 2.1	24.5 ± 3.0	53.3 ± 14.4	31.0 ± 1.9	304.0 ± 50.9	−0.242 ± 0.021	15.1 ± 2.0	10
$Ca_V1.2$:$Ca_V\beta_{2a}$	water 5 min	60.8 ± 1.0	40.0 ± 1.1	34.6 ± 3.9	27.1 ± 0.8	222.8 ± 31.6	−1.344 ± 0.248	9.1 ± 1.8	5
	water 30 min	58.1 ± 1.4	38.3 ± 2.5	37.3 ± 3.0	27.1 ± 2.0	227.3 ± 12.1	−0.785 ± 0.074	11.6 ± 0.7	5
	HotA, 5 min	66.8 ± 0.3	47.5 ± 1.0	28.4 ± 0.7	24.6 ± 1.0	185.7 ± 2.1	−0.734 ± 0.110	10.5 ± 1.5	3
	HotA, 30 min	62.1 ± 0.2	44.4 ± 0.8	33.5 ± 2.3	24.7 ± 0.6	209.5 ± 13.2	−0.531 ± 0.098	9.0 ± 0.5	3
	AID-CAP 400 μM, 5 min	63.7 ± 1.9	41.6 ± 2.5	33.0 ± 2.3	28.9 ± 1.8	215.8 ± 13.2	−0.966 ± 0.154	9.2 ± 1.5	8
	AID-CAP 400 μM, 30 min	57.1 ± 1.6	33.1 ± 2.0	35.0 ± 1.7	28.6 ± 2.0	209.7 ± 9.3	−0.555 ± 0.132	13.0 ± 1.7	8
	AID-CAP 2.8 mM, 5 min	64.6 ± 1.3	52.4 ± 3.1	29.2 ± 3.3	19.3 ± 2.2	172.5 ± 23.4	−0.984 ± 0.142	7.2 ± 0.7	5
	AID-CAP 2.8 mM, 30 min	62.4 ± 2.6	48.1 ± 5.5	30.7 ± 6.0	27.3 ± 1.3	172.2 ± 25.9	−0.465 ± 0.079	10.4 ± 0.7	5
$Ca_V1.2$:$Ca_V\beta_3$	HotA, 5 min	79.2 ± 2.2	79.7 ± 2.3	63.0 ± 2.4			−0.932 ± 0.041	6.7 ± 2.9	5
			61.0 ± 2.4	*38.5 ± 1.5*	*27.9 ± 0.8*	*256.8 ± 10.8*			*5*
	HotA, 30 min	77.0 ± 2.9	78.0 ± 2.7	71.4 ± 4.6			−0.577 ± 0.069	8.6 ± 3.3	5
			56.5 ± 2.0	*42.9 ± 4.4*	*30.0 ± 1.4*	*241.1 ± 14.6*			*5*
	AID-CAP, 5 min	73.2 ± 1.4	75.9 ± 1.2	76.2 ± 4.2			−0.889 ± 0.135	6.3 ± 1.6	6
			57.8 ± 1.2	*48.0 ± 3.7*	*42.0 ± 8.3*	*639.1 ± 238.3*			*6*
	AID-CAP, 30 min	48.3 ± 4.1	66.3 ± 5.0	188.7 ± 30.2			−0.081 ± 0.023	20.5 ± 2.8	6
			ND	*ND*	*ND*	*ND*			
	AID, 5 min	73.4 ± 2.0	76.9 ± 3.1	62.6 ± 7.6			−0.860 ± 0.096	10.4 ± 2.2	7
			54.0 ± 2.7	*40.0 ± 5.2*	*34.1 ± 1.4*	*354.4 ± 119.2*			*7*
	AID, 30 min	49.8 ± 1.9	65.0 ± 4.0	118.2 ± 11.0			−0.116 ± 0.010	21.0 ± 2.0	7
			ND	*ND*	*ND*	*ND*			

[a]Data are expressed as mean values ± SEM; τ values were determined at a holding potential of +20 mV (see Materials and Methods); t_{i300} denotes percent inactivation at 300 ms. I_{max} is the maximal current amplitude. $V_{1/2}$ values for $Ca_V1.2$ and mutants were determined with calcium as the charge carrier. Data were fit using the equation $I = G_{max}(Vm - V_{rev})/(1 + \exp[(V_{1/2} - V_m)/K_a])$, where I is the measured peak current at each V_m, G_{max} is the maximal macroscopic conductance, V_m is the test potential, V_{rev} is the reversal potential, $V_{1/2}$ is the midpoint of activation, and K_a is the slope factor.[29] ND, value not determined. Italic lines highlight double exponential fit values for $Ca_V\beta_3$ experiments.

likely results from the requirement to reduce the degrees of freedom of the highly disordered ligand upon binding.

ITC measurements with AID-CEN and AID-CAP revealed that both peptides bind $Ca_V\beta_{2a}$ with affinities similar to wild-type AID, 5.2 ± 1.5 and 5.1 ± 1.6 nM, respectively (Figure 3B,C, Table 1) but that incorporation of the *m*-xylyl moiety affects the thermodynamic binding parameters of the $Ca_V\beta_{2a}$:AID interaction. Consistent with the incorporation of the *m*-xylyl staple and decrease in random coil as seen by CD (Figure 1), the entropic cost of complex formation was reduced relative to the wild-type for both stapled peptides (ΔS = 2.2 ± 0.5 and −4.6 ± 4.1 cal mol^{-1} K^{-1} for AID-CEN and AID-CAP, respectively). However, this reduction of the unfavorable entropic component was offset by a binding enthalpy reduction (ΔH = −10.2 ± 0.1 and −12.3 ± 1.4 kcal mol^{-1}, AID-CEN and AID-CAP, respectively). Because neither *m*-xylyl staple contributes to the AID:ABP interaction and there are no obvious changes in ABP interaction site contacts (Figure S1A,B), this result appears to be an example of enthalpy−entropy compensation[67] and may originate in the loss of some of the favorable enthalpy of helix formation[68] due to the preordering of the helical structure in the unbound state. Even though the effects of enthalpy−entropy compensation left the binding affinity unaffected, the data demonstrate that the inclusion of the staple was effective at reducing the disorder of the unbound AID as designed.

Stapled AID Peptides Compete with Mutant but Not Wild-type $Ca_V1.2$:$Ca_V\beta_{2a}$ Complexes. Because AID-CAP and AID-CEN had similar affinities for $Ca_V\beta$ but the AID-CAP had the highest amount of helical structure, we focused on testing whether AID-CAP could affect Ca_V function. $Ca_V\beta$ binding to the pore-forming $Ca_V\alpha_1$ subunit AID is known to cause clear changes to channel gating properties, such as the extent and speed of inactivation and the channel activation potential ($V_{1/2}$).[20,45,64] We were concerned that the tight interaction between $Ca_V\alpha_1$ and $Ca_V\beta$ subunits might be difficult

DOI: 10.1021/acschemneuro.6b00454
ACS Chem. Neurosci. 2017, 8, 1313−1326

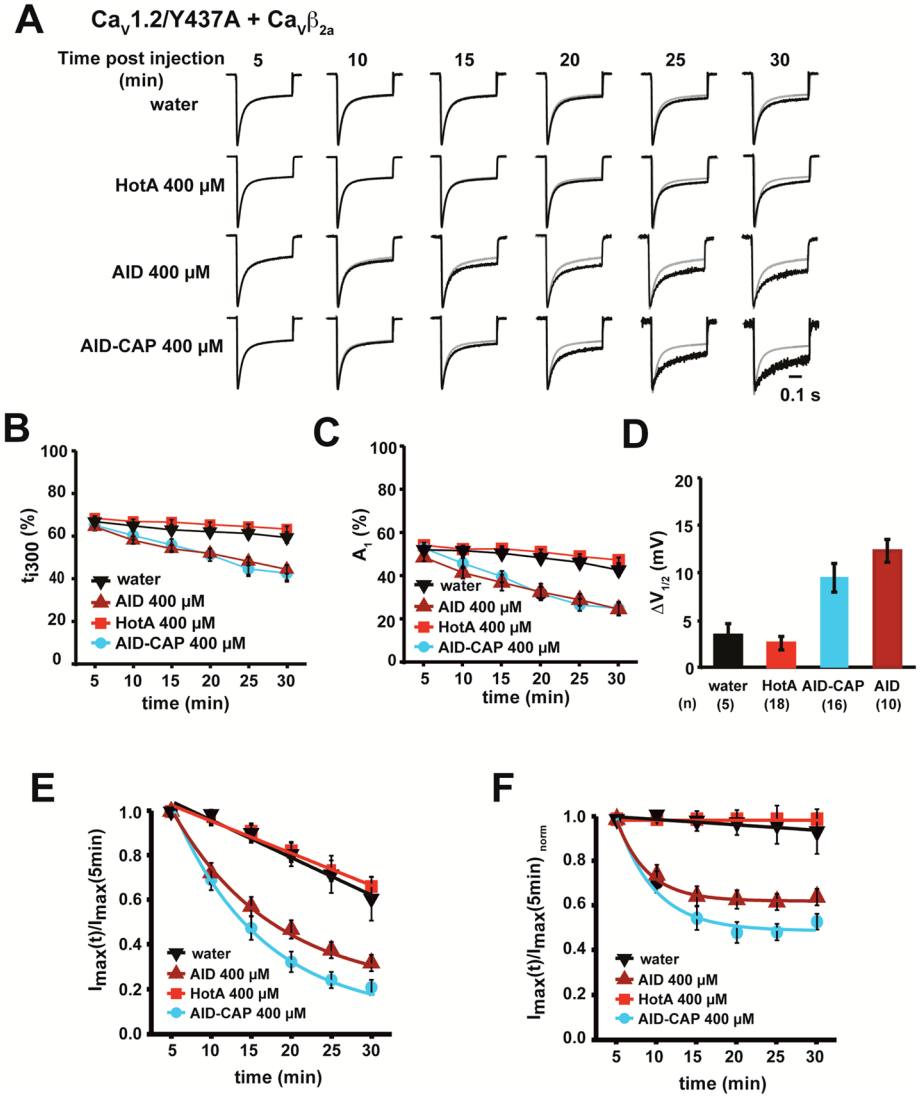

Figure 5. AID-CAP affects Ca$_V$1.2Y437A:Ca$_V\beta_{2a}$ channels. (A) Exemplar normalized I_{Ca} traces at a test potential of +20 mV for *Xenopus* oocytes expressing Ca$_V$1.2-Y437A:Ca$_V\beta_{2a}$ channels recorded after injection of water, 400 μM HotA, 400 μM AID-CAP, or 400 μM AID at the indicated postinjection times. Gray curves at times 10, 15, 20, 25, and 30 min show initial 5 min response. (B) Fractional inactivation after 300 ms (t_{i300}) and (C) A_1, the relative amplitude of the fast inactivation component, for Ca$_V$1.2-Y437A:Ca$_V\beta_{2a}$ currents as a function of postinjection time for water (inverted black triangles), 400 μM HotA (red squares), 400 μM AID (maroon triangles), or 400 μM AID-CAP (blue circles). (D) Change in half maximal activation potential ($\Delta V_{1/2}$) between recordings at 5 and 30 min postinjection. (E) $I_{max}(t)/I_{max}$(5 min) and (F) $I_{max}(t)/I_{max}$(5 min) normalized to $I_{max}(t)/I_{max}$(5 min) of HotA injection as a function of postinjection time. Symbols are as in panels B and C. Lines in panel F show fit to $I(t) = A \exp(-t/\tau) + C$ (exponential) or $I(t) = mt + C$ (linear), where I is the recorded current, A is the amplitude of the loss of current (for exponential fit), m is the slope factor (linear fit), and C is the residual current after 30 min. Results for AID and AID-CAP are statistically different from HotA in all panels ($P < 0.001$). AID and AID-CAP results are not statistically different from each other except in panels E and F where $P < 0.001$.

to compete with an exogenous peptide, particularly because the Ca$_V$1.2:Ca$_V\beta_{2a}$ interaction has been shown to be long-lived unless it is weakened by ABP–AID interface mutations.[69] Hence, we first performed competition experiments using a Ca$_V\alpha_1$ subunit bearing an AID mutation that lowers the Ca$_V\beta$ affinity by ~1000-fold (Y437A, K_d = 5.3 vs 5263 nM for wild-type and Y437A, respectively[45]). To test the ability of AID peptides to interfere with Ca$_V$ function, we measured the response of preassembled, functional, plasma membrane Ca$_V$ complexes expressed in *Xenopus* oocytes to competitor peptides (Figure 4), similar to the approach we used previously to uncover the direct competition between calcium sensor proteins on Ca$_V$s.[70] Two principal inactivation processes govern Ca$_V$ function, voltage-dependent inactivation (VDI)[71,72] and calcium-dependent inactivation (CDI).[25,72,73] Because VDI is essentially absent with Ca$_V\beta_{2a}$[20] and CDI requires Ca$_V\beta$,[64] we measured CDI over the course of 30 min postinjection to monitor functional consequences of AID peptide injection on Ca$_V\beta_{2a}$ containing channels (Figure 4).

One functional signature of the interaction of Ca$_V$1.2 with Ca$_V\beta_{2a}$ is the extent and speed of inactivation, which are more complete and faster, respectively, in the presence of Ca$_V\beta_{2a}$ (Table 2). Prior to peptide injection, Ca$_V$1.2-Y437A:Ca$_V\beta_{2a}$ channels were essentially functionally identical to wild-type Ca$_V$1.2:Ca$_V\beta_{2a}$ channels (Table 2). Within 30 min of injection of 400 μM AID or AID-CAP peptides, we observed substantial and similar changes from both peptides with respect to the extent of channel inactivation 300 ms after activation (t_{i300})

DOI: 10.1021/acschemneuro.6b00454
ACS Chem. Neurosci. 2017, 8, 1313–1326

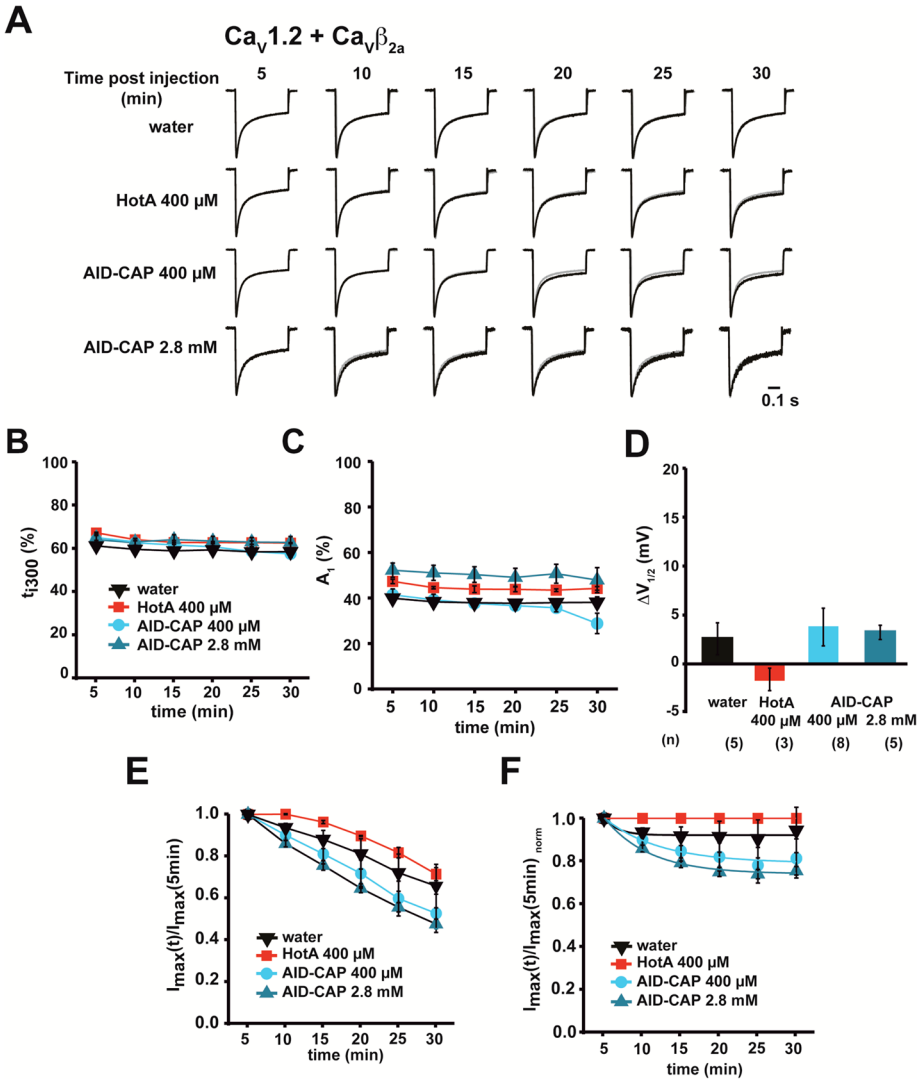

Figure 6. Ca$_V$1.2:Ca$_V\beta_{2a}$ channels resist AID-CAP modulation. (A) Exemplar normalized I_{Ca} traces at a test potential of +20 mV for *Xenopus* oocytes expressing Ca$_V$1.2:Ca$_V\beta_{2a}$ channels recorded after injection of water, 400 μM HotA, 400 μM AID-CAP, or 2.8 mM AID-CAP at the indicated postinjection times. Gray curves at times 10, 15, 20, 25, and 30 min show initial 5 min response. (B, C) Postinjection values of (B) fractional inactivation after 300 ms (t_{i300}) and (C) A_1, the relative amplitude of the fast inactivation component, for Ca$_V$1.2-Y437A:Ca$_V\beta_{2a}$ currents as a function of postinjection time for water (inverted black triangles), 400 μM HotA (red squares), 400 μM AID-CAP (blue circles), or 2.8 mM AID-CAP (teal triangles). (D) Change in half maximal activation potential ($\Delta V_{1/2}$) between recordings 5 and 30 min postinjection. (E) $I_{max}(t)/I_{max}$(5 min) and (F) $I_{max}(t)/I_{max}$(5 min) normalized to HotA injection as a function of postinjection time. Symbols are as in panel B and C. Lines in panel F show fit to $I(t) = A \exp(-t/\tau) + C$ (exponential) or $I(t) = mt + C$ (linear), where I is the recorded current, A is the amplitude of the loss of current (for exponential fit), m is the slope factor (linear fit), and C is the residual current after 30 min. There are no statistically significant differences in the results shown in the panels, except for panels E and F where the AID-CAP 2.8 mM results are statistically significant from Hot A ($P = 0.034$).

(t_{i300} decreased from 64.9% ± 1.9% to 44.8% ± 2.1% and 65.5% ± 1.3% to 43.1% ± 3.7% for AID and AID-CAP, respectively) (Figure 5A–C). In fact, at 30 min after peptide injection, the extent of inactivation was indistinguishable from Ca$_V$1.2 expressed in the absence of Ca$_V\beta$ (t_{i300} = 47.9% ± 1.2%, 44.8% ± 2.1% and 43.1% ± 3.7% for no Ca$_V\beta$, AID (30 min), and AID-CAP (30 min), respectively), suggesting that the peptides had interfered completely with Ca$_V\beta$ binding. By contrast, injection of an AID mutant peptide in which the three most important residues for binding to Ca$_V\beta$ were mutated to alanine (Y437A/W440A/I441A, termed "HotA"[45]) showed no specific effects on fractional inactivation and had effects indistinguishable from water injection (Figure 5) (t_{i300} decreased from 68.8% ± 1.0% to 63.7% ± 1.3% and 67.2% ± 1.9% to 59.8% ± 2.6% for HotA and water, respectively, Figure 5 and Table 2). In addition to the t_{i300} changes, the fraction of the fast inactivation component decreased after injection of either AID or AID-CAP to levels similar to Ca$_V$1.2 expressed without a Ca$_V\beta$ subunit (Figure 5C).

A second functional signature of the interaction of Ca$_V\beta_{2a}$ with Ca$_V$1.2 is a hyperpolarizing shift of ~10 mV in the channel activation ($V_{1/2}$ = 18.1 ± 1.0 and 8.1 ± 1.2 mV for Ca$_V$1.2 without and with Ca$_V\beta_{2a}$, respectively, Table 2). In Ca$_V$1.2 Y437A:Ca$_V\beta_{2a}$ channels, competition with both the AID and AID-CAP peptides reduced this effect of Ca$_V\beta$ on channel activation ($V_{1/2}$ = 15.1 ± 2.0 and 16.9 ± 1.0 mV for AID and AID-CAP, respectively) (Figure 5D, Table 2). By contrast, oocytes coexpressing Ca$_V$1.2-Y437A:Ca$_V\beta_{2a}$ that were injected with either water or the HotA peptide did not show any changes in gating characteristics. These observations are

DOI: 10.1021/acschemneuro.6b00454
ACS Chem. Neurosci. 2017, 8, 1313–1326

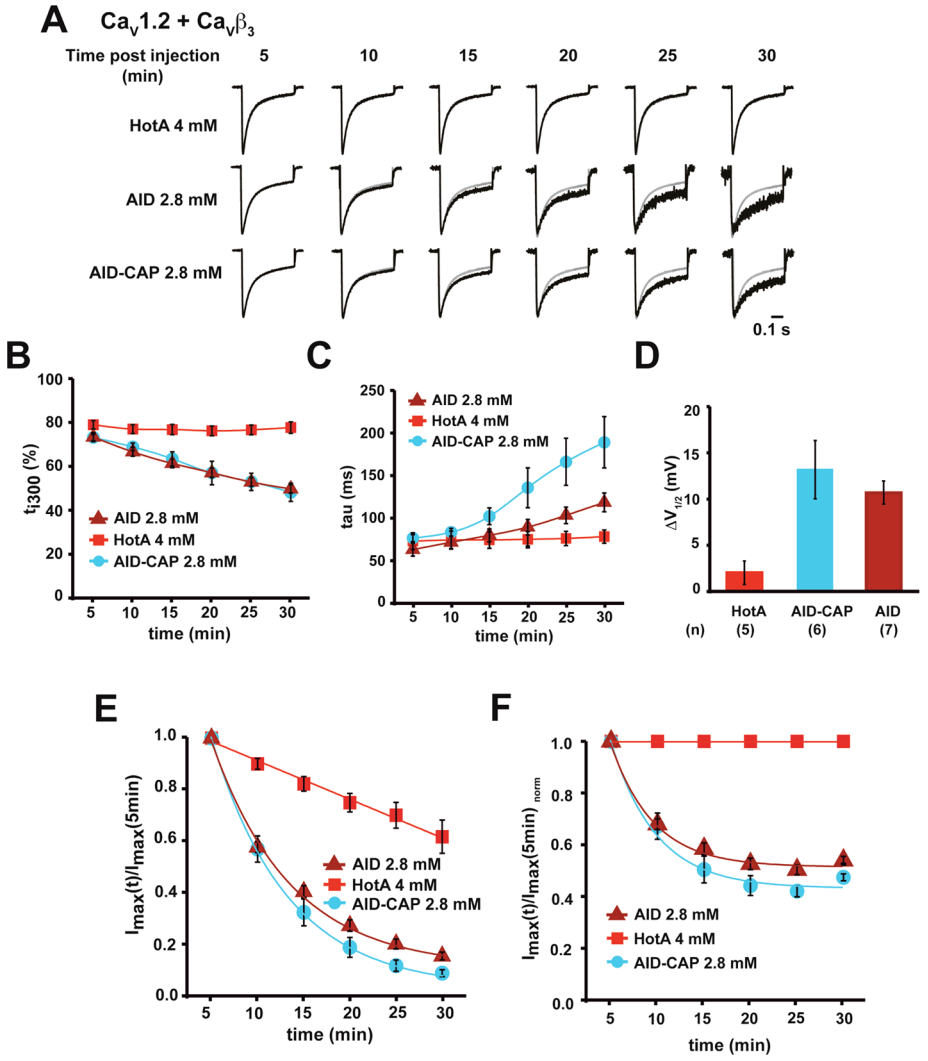

Figure 7. AID-CAP affects Ca$_V$1.2:Ca$_V\beta_3$ channels. (A) Exemplar normalized I_{Ca} traces at a test potential of +20 mV for *Xenopus* oocytes expressing Ca$_V$1.2:Ca$_V\beta_3$ channels recorded after injection of 4 mM HotA, 2.8 mM AID-CAP, or 2.8 mM AID at the indicated postinjection times. Gray curves at times 10, 15, 20, 25, and 30 min show initial 5 min response. (B, C) Postinjection values of (B) fractional inactivation after 300 ms (t_{i300}) and (C) t, the fast inactivation time constant of Ca$_V$1.2:Ca$_V\beta_3$ currents, as a function of postinjection time for 4 mM HotA (red squares), 2.8 mM AID (maroon triangles), or 2.8 mM AID-CAP (blue circles). (D) Change in half maximal activation potential ($\Delta V_{1/2}$) between recordings 5 and 30 min postinjection. (E) $I_{max}(t)/I_{max}$(5 min) and (F) $I_{max}(t)/I_{max}$(5 min) normalized to HotA injection as a function of postinjection time. Symbols are as in panels B and C. Lines in panel F show fit to $I(t) = A\exp(-t/\tau) + C$ (exponential) or $I(t) = mt + C$ (linear), where I is the recorded current, A is the amplitude of the loss of current (for exponential fit), m is the slope factor (linear fit), and C is the residual current after 30 min. Because of the switch in inactivation behavior, to facilitate comparisons, values from monoxponential fits of the channel kinetics were used for panel C. Results for AID and AID-CAP are statistically different from HotA in all panels ($P < 0.001$ for panels B, E, and F; $P < 0.05$ for panels C and D). AID and AID-CAP results are not statistically different from each other except in panels C, E, and F where $P < 0.001$.

consistent with the notion that AID and AID-CAP peptide injection counteracted the effect of Ca$_V\beta_{2a}$ on the voltage-dependency of channel activation and suggest that the observed effects arise from disruption of the Ca$_V$1.2:Ca$_V\beta_{2a}$ interaction.

Recordings from Ca$_V$1.2-Y437A:Ca$_V\beta_{2a}$ expressing oocytes challenged by AID or AID-CAP also showed consistently higher rundown, compared to recordings from water or HotA peptide injected oocytes (Figure 5E and Table 2). This increased rundown may reflect some enhanced internalization of channel once the Ca$_V$1.2:Ca$_V\beta$ interaction is lost or possible inhibition of the formation of new complexes. Subtraction of the water-injected baseline revealed that the AID and AID-CAP induced rundown of I_{max} reached steady state on the time scale of minutes (Figure 5F) and that the AID-CAP peptide was more potent than the unstapled wild-type. The rundown process could be well fit by a single exponential (Figure 5F) (τ = 5.3 ± 0.9 and 4.1 ± 0.4 min for AID and AID-CAP, respectively). All of the observed characteristic changes caused by AID and AID-CAP injection are consistent with a disruption of the Ca$_V$1.2:Ca$_V\beta_{2a}$ interaction.

Given that the AID-CAP peptide performed better than the AID, we next asked whether AID-CAP could compete with Ca$_V\beta_{2a}$ bound to an unaltered channel. Contrasting the results with Ca$_V$1.2-Y437A, the effects of 400 μM AID-CAP injection into wild-type Ca$_V$1.2 expressing oocytes were not different from the effects seen with water or similar concentration injections of HotA on Ca$_V$1.2-Y437A:Ca$_V\beta_{2a}$. Increasing the injected AID-CAP concentration to 2.8 mM did not cause functional effects that were different from the negative controls with the exception of inducing a slight increase in channel

DOI: 10.1021/acschemneuro.6b00454
ACS Chem. Neurosci. 2017, 8, 1313−1326

rundown (Figure 6). Thus, unlike the situation in which the AID:ABP interaction is weakened by the Y437A mutation in the $Ca_V1.2$ α_1-subunit AID, native $Ca_V1.2$:$Ca_V\beta_{2a}$ complexes appear to be sufficiently stable to resist kinetic competition by the injected peptides.

Stapled AID Peptides Compete with Functional $Ca_V1.2/Ca_V\beta_3$ Complexes in Oocytes. $Ca_V\beta_{2a}$ bears an N-terminal palmitoylation site[74] that anchors it to the plasma membrane making it different from other $Ca_V\beta$ isoforms. This membrane tethering should increase the effective concentration[75] of the AID:ABP interaction and could thwart the ability of AID peptides to compete with the native AID:ABP interaction. To test this idea, we examined whether AID and AID-CAP peptides could affect wild-type $Ca_V1.2$ coexpressed with nonpalmitoylated isoform $Ca_V\beta_3$ that shares a conserved structure and ABP-AID interface with $Ca_V\beta_{2a}$.[45,46] By strong contrast with the $Ca_V1.2$:$Ca_V\beta_{2a}$ results (Figure 6), injection of AID or AID-CAP into oocytes expressing $Ca_V1.2$:$Ca_V\beta_3$ channels at the maximal peptide concentration that was ineffective against $Ca_V1.2$:$Ca_V\beta_{2a}$ channels (2.8 mM, Figure 7) resulted in a striking change of the channel properties compared to the control HotA peptide (Figure 7A, Table 2). Over the course of 30 min, competition with AID and AID-CAP decreased the extent of inactivation (t_{i300} from 73.4% ± 2.0% to 49.8% ± 1.9% and from 73.2% ± 1.5% to 48.3% ± 4.1%, respectively, Figure 7B), prolonged τ of inactivation (Figure 7C), and shifted the activation $V_{1/2}$ (from 6.3 ± 1.6 to 20.5 ± 2.8 mV and from 10.4 ± 2.2 to 21.0 ± 2.0 mV for AID-CAP and AID, in contrast to HotA, from 6.7 ± 2.9 to 8.6 ± 3.3 mV Figure 7D). Following injection with both the AID-CAP and AID peptides, there was also a clear change in channel inactivation kinetics, which changed from one having two components to a monoexponential process. Similar to the $Ca_V1.2$-Y437A:$Ca_V\beta_{2a}$ experiments, injection of AID and AID-CAP peptides resulted in strongly increased current rundown, consistent with a loss of active channels on the plasma membrane (Figure 7E). All of these functional changes are consistent with the near complete disruption of the $Ca_V1.2\alpha_1$:$Ca_V\beta_3$ interaction and are absent in currents from oocytes expressing $Ca_V1.2$:$Ca_V\beta_3$ challenged with the HotA peptide. The similar performance of the AID and AID-CAP peptides matches their comparable affinities for $Ca_V\beta$ (Figure 3 and Table 1). There is a slight advantage for the AID-CAP version that suggests that the peptide staple improves the performance of the peptide in a cellular setting (Figure 7).

Measurement of the time constant for the loss of channels by fitting to a single exponential yields τ = 5.3 ± 0.7 and 4.6 ± 0.4 min for AID-CAP and AID, respectively. These values are notably similar to those measured for $Ca_V1.2$ Y437A:$Ca_V\beta_{2a}$ complexes (5.3 ± 0.9 and 4.1 ± 0.4 min, respectively, Figure 7F) and are within a factor of 3 of the reported k_{off} for dissociation of purified $Ca_V2.2$ I–II loop peptide and $Ca_V\beta_{2b}$ (τ = 2.1 min).[44] These observations, together with the similar binding properties of all AID and $Ca_V\beta$ isoforms,[45] suggest that the functional effects we observe are driven by dissociation of $Ca_V\beta$ from the channel. Taken together, our data demonstrate that it is possible to use exogenous AID peptides to disrupt $Ca_V\alpha$:$Ca_V\beta$ interactions. Differences in the labile nature of the AID:$Ca_V\beta$ interaction lead to $Ca_V\beta$ isoform-specific effects even though the target AID:ABP interactions are strictly conserved.

DISCUSSION

The function, regulation, and biogenesis of many VGIC superfamily members rely on the formation of protein–protein complexes between VGIC pore-forming and cytoplasmic subunits.[1,76] Well-studied examples of how this class of protein–protein interactions can affect VGIC biophysical properties and cellular targeting have been elaborated for Ca_V1 and Ca_V2 pore-forming subunits with $Ca_V\beta$[20,23,45−48] and the interaction of Kv1 and Kv4 voltage gated potassium channels with either Kvβ[4,77] or KChIPs,[4,78] respectively. In particular, application of Ca_V1 AID peptides to channel containing membrane patches has been reported to modulate $Ca_V1.2$ channels in a manner consistent with competition of the $Ca_V\alpha_1$:$Ca_V\beta$ interaction[55] and comprehensive structural and functional studies have shown that cortisone can modulate Kv1 channels by competing with the K_V1–Kvβ interaction.[6,7] These initial studies suggest that antagonists of the protein–protein interactions between pore-forming and cytoplasmic VGIC components may offer an alternative strategy to control channel function that contrasts the classical approaches that target the pore-forming subunit.[19,50−52,79]

Targeting protein–protein interactions remains challenging.[14,16] Nevertheless, notable successes have been made in developing protein–protein interaction antagonists for a variety of cellular targets such as Bcl-X_L, p53, and estrogen receptors.[14−17] Despite the many successes with intracellular targets, there has been little successful development reported regarding VGIC protein–protein interaction antagonists. Two studies have detailed the search for compounds that would affect $Ca_V\alpha$–$Ca_V\beta$[53] and Kv4–KChIP interactions,[80] but neither validated the reported compounds as authentic protein–protein interaction antagonists. Given such lack of progress targeting ion channel protein–protein interactions as a point of pharmacological intervention and questions about the degree to which interactions between pore-forming and cytoplasmic subunits may be labile, there has been reasonable skepticism about whether targeting such interactions can be a viable strategy to control channel function in cellular settings.[12,19] Our studies here, using a classic paradigm for cytoplasmic subunit modulation, that of the $Ca_V\alpha_1$:$Ca_V\beta$ interaction, now validate the concept of using protein–protein antagonists to control a VGIC and should open a path to further development of this type of strategy to control channel function.

Protein–protein interactions involving the binding of an α-helix to a partner protein represent one of the most attractive architectures for protein–protein interaction antagonist development[15] as the interaction surface is limited and there are a variety of strategies for improving the properties of the α-helical partner. The AID:ABP interaction presents an example of this sort of interaction in an ion channel complex. The α-helical element of the complex, the AID, lacks structure in its unbound state[45,47,64,65] and binds to a well-defined $Ca_V\beta$ cleft, the ABP, that undergoes minimal conformational change.[46−48] Because α-helix stabilization strategies have proven successful for targeting many protein–protein interactions mediated by a similar general architecture[15] and the binding energy of the AID:ABP is focused into a hotspot in the center of the AID helix,[45] we reasoned that pursuing a stapled peptide strategy[58] to enhance the stability of the AID helix might provide a first step in the development of $Ca_V\beta$-directed inhibitors of Ca_V function.

DOI: 10.1021/acschemneuro.6b00454
ACS Chem. Neurosci. 2017, 8, 1313−1326

Incorporation of an *m*-xylyl staple, a strategy used previously to stabilize the protease inhibitor calpastatin[59] and β-catenin,[60] enhanced AID helix formation when placed at either N-terminal (AID-CAP) or central (AID-CEN) positions (Figure 1C). The AID-CAP configuration proved superior for inducing helical content. We attribute this effect to the stabilization of an engineered helix cap by the *m*-xylyl staple (Figure S1C) and the importance of helix nucleation.[81,82] Our crystallographic studies show that neither *m*-xylyl staple position altered the way the AID peptides bind $Ca_V\beta$ (Figure 2). As anticipated, *m*-xylyl staple incorporation reduced the entropic penalty of $Ca_V\beta$ binding (Table 1) in a manner consistent with reduction of disorder in the unbound AID. Nevertheless, despite this effect, lack of interference of the staples with $Ca_V\beta$ complex formation, and lack of conformational change in the $Ca_V\beta$ ABP, there was a concomitant reduction in the large enthalpic gain of complex formation that resulted in no measurable change in $Ca_V\beta$ binding affinity between the unconstrained and stapled AIDs (Table 1). Such entropy−enthalpy compensation effects are not uncommon in protein−ligand recognition and design efforts.[67] In the case of the stapled AIDs, the ordering of the helical conformation may have traded away some of the gain in favorable enthalpy associated with the formation of helical backbone interactions[68] that would otherwise be associated with the binding reaction. The structural information obtained here should enable strategies using other cross-linking sites or the combination of multiple staples to provide a path toward more efficacious peptide-based $Ca_V\alpha$:$Ca_V\beta$ protein−protein interaction inhibitors. Notably, even in the absence of affinity enhancement effects, the helical staples may offer advantages, as our cell-based assays indicated that the stapled peptide outperformed the unstapled AID (Figures 5 and 7). Hence, there may be multiple layers of benefit to helix stabilization in a cellular context that go beyond the effects on binding affinity.

Two challenges to targeting the AID:ABP interaction are competition with a nanomolar native interaction[45] and the fact that the AID:ABP interface comprises well-conserved interactions among the isoforms of both partners.[45] Despite these challenges, our functional studies showed that injection of either wild-type AID or AID-CAP into *Xenopus* oocytes expressing $Ca_V1.2$-Y437A:$Ca_V\beta_{2a}$ or $Ca_V1.2$:$Ca_V\beta_3$ channel complexes resulted in biophysical changes that were consistent with loss of $Ca_V\beta$ modulation and binding. Such changes were absent for $Ca_V1.2$:$Ca_V\beta_{2a}$ channels in which the $Ca_V\beta$ component is anchored to the membrane via palmitoylation.[74] The biophysical parameter changes were also accompanied by a reduction of channels at the cell membrane as indicated by the changes in the I_{max} parameter. Notably, such changes could also be observed for $Ca_V1.2$:$Ca_V\beta_{2a}$, although to a lesser extent than with $Ca_V1.2$-Y437A:$Ca_V\beta_{2a}$ or $Ca_V1.2$:$Ca_V\beta_3$, suggesting that the peptides may not only affect channels at the membrane but inhibit the formation or membrane incorporation of newly assembled channels or may influence channel destruction by the ERAD system.[30] Interestingly, the time constants measured for the I_{max} changes are close to the intrinsic dissociation rates reported for the AID−$Ca_V\beta$ interaction[44] and suggest that some of the competitive effects of the peptides may be governed by the intrinsic dissociation rates of $Ca_V\beta$ from the pore-forming subunit. Together, our data demonstrate that the AID:ABP interaction can be targeted effectively in a cellular context. Importantly, despite the high similarity in the residues that contribute to the AID:ABP interface and the corresponding similar interaction affinities for AID−$Ca_V\beta$ pairs,[45] our findings show that it is possible to achieve some degree of isoform selective specificity. This selectivity appears to originate in factors outside of the ABP−AID interface that contribute to the diverse functional effects of the different $Ca_V\beta$ isoforms, that likely affect how $Ca_V\beta$ engages the channel, and that are related to the $Ca_V\beta$ off rate. Thus, our studies with stapled AID peptides show that it is possible to antagonize a paradigmatic protein−protein interaction central to VGIC function, for Ca_V current regulation and achieve specificity between different $Ca_V\beta$ isoforms.

VGICs have well-established important roles in the generation of bioelectrical signals in excitable tissues such as brain, heart, and muscle[1] and also have an emerging set of "nonclassical" roles in insulin secretion,[83] cancer,[84−86] and gene regulation.[87,88] Because of these diverse functions and a general lack of specific means for controlling channel function, there remains a need to develop new molecular tools that can be used to probe VGIC biology.[51,89,90] Due to the importance of protein−protein interactions between pore-forming and cytoplasmic VGIC subunits for the biogenesis and trafficking of many VGICs, further development of such VGIC protein−protein interaction antagonists may open new means to study the dynamics of channel complexes, the steps associated with channel assembly, and the roles of these processes in native setting excitable tissues such as muscles and neurons.

MATERIALS AND METHODS

Molecular Biology. Human $Ca_V1.2$ (α_1C77, GenBank Z34815), human $Ca_V1.2$-Y437A, rat $Ca_V\beta_{2a}$ (GenBank NM_053851), $Ca_V\beta_3$ (GenBank NM_001101715), and $Ca_V\alpha_2\delta$-1 (GenBank NM_00182276) were used for two-electrode voltage clamp experiments in *Xenopus* oocytes. For constructing $Ca_V1.2$-Y437A, the mutation in position 437 of $Ca_V1.2$ was introduced by SOE-PCR (Splicing by Overlap-PCR). Briefly, the I−II loop cDNA sequence of $Ca_V1.2$ was PCR amplified with overlapping mutagenesis primers in separate PCR reactions using pcDNA3.1-$Ca_V1.2$ as template. The two separate PCR products were then used as templates for a final PCR reaction with flanking primers to connect the nucleotide sequences. This fragment was then *Hpa*I/*Ppu*MI digested and cloned into the respective sites of pcDNA3.1-$Ca_V1.2$.

Protein Expression and Purification. $Ca_V\beta_{2a}$ expression and purification were done as previously described.[45] For complex formation with stapled peptides, 155 uM $Ca_V\beta_{2a}$ in buffer A (150 mM KCl, 1 mM TCEP, pH 7.4, 10 mM HEPES/KOH, pH 7.4) was mixed with an equal volume of peptide in buffer A, creating a molar ratio of protein/peptide of 1:1.2. Unbound peptide was removed using a Superdex200 HR10/30 gel filtration column run in buffer A. The $Ca_V\beta_{2a}$/peptide complex was concentrated (Amicon filter, MWCO 10 kDa) to 8 mg/mL as determined by absorbance.[91]

Peptide Synthesis and Purification. All the AID peptides were synthesized using an automated peptide synthesizer (0.1 mmol scale). Fmoc-solid phase peptide synthesis was employed on Chemmatrix Rinkamde resin (substitution level ∼0.5 mmol/g). Deprotection was performed with 20% 4-methylpiperidine in DMF, and coupling reactions were done in a mixture of Fmoc-amino acid (5 equiv), HCTU (4.95 equiv), and DIPEA (10 equiv) in DMF at 70 °C for 5 min. The peptide was cleaved from the resin by treatment with the cleavage cocktail (TFA/EDT/thioanisole = 95:2.5:2.5), and the crude product was obtained by cold ether precipitation after removal of TFA. The crude peptide was purified by reverse phase (RP)-HPLC C4 column and lyophilized.

Peptide Cross-Linking. Peptide cross-linking was performed as described previously.[59] Briefly, a solution of cysteine containing peptide (0.1 mM) was incubated with TCEP (1.5 equiv) in NH_4HCO_3 buffer (100 mM, pH = 8.0) for 30 min. Then *m*,*m*′-dibromoxylene solution (2 or 3 equiv, 1 mM in DMF) was added and stirred at room temperature. The reaction progress was monitored by

DOI: 10.1021/acschemneuro.6b00454
ACS Chem. Neurosci. 2017, 8, 1313−1326

mass spectrometry. When the reaction was complete, the reaction mixture was quenched by 1 M HCl solution to acidic pH (pH 3 or 4) and purified by RP-HPLC.

Crystallization and Refinement. The $Ca_V\beta_{2a}$/ASPL complex was crystallized by hanging drop vapor diffusion at 4 °C by mixing equal volumes of protein in buffer A and well solution containing 1.5−1.7 M $(NH_4)_2SO_4$, 5 mM β-mercaptoethanol, and 0.1 M HEPES, pH 7. The $Ca_V\beta_{2a}$/CSPE complex was crystallized by hanging drop vapor diffusion at 4 °C by mixing equal volumes of protein in buffer A and well solution containing 34−37% PEG400, 0.1 M $MgCl_2$, and 0.1 M MES, pH 6.3. After flash-freezing in well solution plus 20% glycerol, diffraction data were collected at Beamline 8.3.1 (Advanced Light Source, Lawrence Berkeley National Laboratories), indexed using MOSFLM 7.0.4,[92] and scaled using SCALA.[93] Molecular replacement with PHASER[94] using a model derived from 1T3S yielded starting phases. The initial model was improved by iterative cycles of manual building in COOT[95] and refinement against native data using Refmac5.[96] TLS-tensors were added in the final cycle of refinement. Data collection and final model refinement statistics are summarized in Table S1.

Circular Dichroism. Circular dichroism spectra were measured in a 2 mm path length quartz cuvette (Hellma), 50 mM KCl, and 10 mM KH_2PO_4/K_2HPO_4, pH 7.3, using an Aviv model 215 spectropolarimeter (Aviv Biomedical) equipped with a Peltier temperature controller. Wavelength scans from 320 to 190 nm were taken at 4 °C. Each point was determined in triplicate from the same sample and subtracted by the average of a triplicate buffer scan. Each sample was checked for purity by HPLC. Molar ellipticity was calculated as follows: $\theta = 100(\Delta m)/(Cnl)$, where Δm is the CD signal in millidegrees after buffer subtraction, C is the millimolar peptide concentration, n is the number of residues in the peptide, and l is the cuvette path length in centimeters.

Isothermal Calorimetry. Titrations were performed at 15 °C using a VP-ITC microcalorimeter (MicroCal). Samples were dialyzed overnight at 4 °C (Slide-A-Lyzer, 2 kDa molecular weight cutoff, Thermo Scientific) against 150 mM KCl and 10 mM potassium phosphate, pH 7.3. After 30 min centrifugation at 40 000 rpm at 4 °C, protein concentrations were determined by absorbance at 280 nm.[91] All samples were degassed for 5 min prior to loading into the calorimeter. $Ca_V1.2$ $Ca_V\beta_{2a}$ core at a concentration of 2 μM was titrated with 20 μM modified or unmodified AID peptide with one 4 μL injection followed by 29 injections of 10 μL of titrant. To correct the baseline, heat of dilution from titrations of injectant into buffer was subtracted. Data were processed with MicroCal Origin 7.0 using a single site binding model.

Electrophysiology. Details of two-electrode voltage clamp have been described previously.[64] In short, linearized cDNA was translated into capped mRNA using the T7 mMessenger kit (Ambion). Fifty nanoliters of a mRNA mixture containing an equimolar ratio of $Ca_V\alpha_1$ and $Ca_V\alpha_2\delta$-1 and a lower amount of $Ca_V\beta$ were microinjected into *Xenopus* oocytes 48−72 h prior to recording. After injection, the oocytes were kept at 18 °C in ND96 medium supplemented with penicillin (100 U mL^{-1}) and streptomycin (100 μg mL^{-1}). Prior studies established that with injections of an equimolar ratio of $Ca_V\alpha_1$ and $Ca_V\beta$ RNA, there is an excess of free $Ca_V\beta$.[64] To avoid an excess of free $Ca_V\beta$ in the cytoplasm, the optimal $Ca_V\alpha_1/Ca_V\beta$ RNA ratio was determined for each RNA preparation. Different $Ca_V\alpha_1/Ca_V\beta$ molar ratios were titrated for every RNA preparation, and the highest $Ca_V\alpha_1/Ca_V\beta$ RNA ratio at which the channel currents displayed the same extent and speed of inactivation as oocytes injected with equimolar ratio of $Ca_V\alpha_1/Ca_V\beta$ was used for peptide injection experiments (1:10 to 1:100 for $Ca_V\beta_{2a}$:$Ca_V1.2$; 1:1 for $Ca_V\beta_3$:$Ca_V1.2$).

For experiments that involved peptide injections into oocytes, 5 min before the first recording, 50 nL of a mixture of 0.1 M BAPTA and the test substance (peptide or water) was injected. Recording solutions contained 40 mM $Ca(NO_3)_2$, 50 mM NaOH, 1 mM KOH, and 10 mM HEPES, adjusted to pH 7.4 using HNO_3. Electrodes were filled with 3 M KCl and had resistances of 0.3−2.0 MΩ. Leak currents were subtracted using a P/4 protocol. Currents were analyzed with Clampfit 8.2 (Axon Instruments). All results are from at least two independent oocyte batches. The t_{i300} values were calculated from normalized currents at +20 mV and represent the percentage of inactivation after 300 ms. Inactivation τ values at +20 mV, G_{max}, K_a, $V_{1/2}$, and V_{rev} were calculated as described.[64]

Statistical Analysis. Data are expressed as mean ± SEM. Statistical differences between samples were determined using one-way analysis of variance or Kruskal−Wallis one way analysis of variance on ranks (when data were not normally distributed) and two-way analysis of variance associated with a Holm−Sidak post hoc test when needed. A value of $p < 0.05$ was considered significant.

■ ASSOCIATED CONTENT

Supporting Information

The Supporting Information is available free of charge on the ACS Publications website at DOI: 10.1021/acschemneuro.6b00454.

Structures of $Ca_V\beta_{2a}$:stapled peptide complexes and crystallographic data (PDF)

Accession Codes

Coordinates and structure factors for have been deposited for $Ca_V\beta_{2a}$:$Ca_V1.2$ AID-CAP (5V2P) and $Ca_V\beta_{2a}$:AID-CEN (5V2Q) and will be immediately available upon publication.

■ AUTHOR INFORMATION

Corresponding Author

*E-mail: daniel.minor@ucsf.edu.

ORCID

Daniel L. Minor Jr.: 0000-0002-5998-4214

Author Contributions

F.F. and M.C. contributed equally. M.C., F.F., H.J., W.F.D., and D.L.M. conceived the study and designed the experiments. F.F., M.C., H.J., C.H.R., L.P., F.A.A., and N.D.R. performed the experiments. F.F. purified, crystallized, and determined the structures of AID-$Ca_V\beta$ complexes, performed the CD experiments, and analyzed the data. F.F., M.C., F.A.A., and N.D.R. performed electrophysiological experiments and analyzed the data. H.J. and W.F.D. designed and synthesized the peptides. D.L.M analyzed the data and provided guidance and support throughout. F.F., M.C., H.J., F.A.A., B.E.F., W.F.D., and D.L.M. wrote the paper.

Notes

The authors declare no competing financial interest.

■ ACKNOWLEDGMENTS

We thank M. Grabe for insightful discussions and comments on the manuscript. This work was supported by NIH Grant R01-HL080050 to D.L.M. and Grant R01-GM54616 to W.F.D. and Austrian Science Fund (FWF) Grant W01101 to B.E.F.

■ REFERENCES

(1) Hille, B. (2001) *Ion Channels of Excitable Membranes*, 3rd ed., Sinauer Associates, Inc., Sunderland, MA.

(2) Yu, F. H., Yarov-Yarovoy, V., Gutman, G. A., and Catterall, W. A. (2005) Overview of molecular relationships in the voltage-gated ion channel superfamily. *Pharmacol Rev. 57*, 387−395.

(3) Simms, B. A., and Zamponi, G. W. (2012) Trafficking and stability of voltage-gated calcium channels. *Cell. Mol. Life Sci. 69*, 843−856.

(4) Pongs, O., and Schwarz, J. R. (2010) Ancillary subunits associated with voltage-dependent K+ channels. *Physiol. Rev. 90*, 755−796.

(5) Schwappach, B. (2008) An overview of trafficking and assembly of neurotransmitter receptors and ion channels (Review). *Mol. Membr. Biol. 25*, 270−278.

DOI: 10.1021/acschemneuro.6b00454
ACS Chem. Neurosci. 2017, 8, 1313−1326

(6) Pan, Y., Levin, E. J., Quick, M., and Zhou, M. (2012) Potentiation of the Kv1 family K(+) channel by cortisone analogues. *ACS Chem. Biol. 7*, 1641−1646.
(7) Pan, Y., Weng, J., Kabaleeswaran, V., Li, H., Cao, Y., Bhosle, R. C., and Zhou, M. (2008) Cortisone dissociates the Shaker family K+ channels from their beta subunits. *Nat. Chem. Biol. 4*, 708−714.
(8) Yang, T., Suhail, Y., Dalton, S., Kernan, T., and Colecraft, H. M. (2007) Genetically encoded molecules for inducibly inactivating CaV channels. *Nat. Chem. Biol. 3*, 795−804.
(9) Yang, T., He, L. L., Chen, M., Fang, K., and Colecraft, H. M. (2013) Bio-inspired voltage-dependent calcium channel blockers. *Nat. Commun. 4*, 2540.
(10) Rouwette, T., Avenali, L., Sondermann, J., Narayanan, P., Gomez-Varela, D., and Schmidt, M. (2015) Modulation of nociceptive ion channels and receptors via protein-protein interactions: implications for pain relief. *Channels 9*, 175−185.
(11) Subramanyam, P., and Colecraft, H. M. (2015) Ion channel engineering: perspectives and strategies. *J. Mol. Biol. 427*, 190−204.
(12) Kohout, S. C., and Isacoff, E. Y. (2008) To dislodge an enzyme from an ion channel, try steroids. *Nat. Chem. Biol. 4*, 650−651.
(13) Laraia, L., McKenzie, G., Spring, D. R., Venkitaraman, A. R., and Huggins, D. J. (2015) Overcoming Chemical, Biological, and Computational Challenges in the Development of Inhibitors Targeting Protein-Protein Interactions. *Chem. Biol. 22*, 689−703.
(14) Wells, J. A., and McClendon, C. L. (2007) Reaching for high-hanging fruit in drug discovery at protein-protein interfaces. *Nature 450*, 1001−1009.
(15) Azzarito, V., Long, K., Murphy, N. S., and Wilson, A. J. (2013) Inhibition of alpha-helix-mediated protein-protein interactions using designed molecules. *Nat. Chem. 5*, 161−173.
(16) Milroy, L. G., Grossmann, T. N., Hennig, S., Brunsveld, L., and Ottmann, C. (2014) Modulators of protein-protein interactions. *Chem. Rev. 114*, 4695−4748.
(17) Cromm, P. M., Spiegel, J., and Grossmann, T. N. (2015) Hydrocarbon stapled peptides as modulators of biological function. *ACS Chem. Biol. 10*, 1362−1375.
(18) Findeisen, F., and Minor, D. L., Jr. (2010) Progress in the structural understanding of voltage-gated calcium channel (CaV) function and modulation. *Channels 4*, 459−474.
(19) Zamponi, G. W., Striessnig, J., Koschak, A., and Dolphin, A. C. (2015) The Physiology, Pathology, and Pharmacology of Voltage-Gated Calcium Channels and Their Future Therapeutic Potential. *Pharmacol. Rev. 67*, 821−870.
(20) Buraei, Z., and Yang, J. (2010) The {beta} Subunit of Voltage-Gated Ca2+ Channels. *Physiol. Rev. 90*, 1461−1506.
(21) Buraei, Z., and Yang, J. (2013) Structure and function of the beta subunit of voltage-gated Ca(2)(+) channels. *Biochim. Biophys. Acta, Biomembr. 1828*, 1530−1540.
(22) Van Petegem, F., and Minor, D. L. (2006) The structural biology of voltage-gated calcium channel function and regulation. *Biochem. Soc. Trans. 34*, 887−893.
(23) Wu, J., Yan, Z., Li, Z., Yan, C., Lu, S., Dong, M., and Yan, N. (2015) Structure of the voltage-gated calcium channel Cav1.1 complex. *Science 350*, aad2395.
(24) Dolphin, A. C. (2013) The alpha2delta subunits of voltage-gated calcium channels. *Biochim. Biophys. Acta, Biomembr. 1828*, 1541−1549.
(25) Ben-Johny, M., and Yue, D. T. (2014) Calmodulin regulation (calmodulation) of voltage-gated calcium channels. *J. Gen. Physiol. 143*, 679−692.
(26) Fang, K., and Colecraft, H. M. (2011) Mechanism of auxiliary beta-subunit-mediated membrane targeting of L-type (Ca(V)1.2) channels. *J. Physiol. 589*, 4437−4455.
(27) Bichet, D., Cornet, V., Geib, S., Carlier, E., Volsen, S., Hoshi, T., Mori, Y., and De Waard, M. (2000) The I-II loop of the Ca2+ channel alpha1 subunit contains an endoplasmic reticulum retention signal antagonized by the beta subunit. *Neuron 25*, 177−190.
(28) Bourdin, B., Marger, F., Wall-Lacelle, S., Schneider, T., Klein, H., Sauve, R., and Parent, L. (2010) Molecular determinants of the CaVbeta-induced plasma membrane targeting of the CaV1.2 channel. *J. Biol. Chem. 285*, 22853−22863.
(29) Kanevsky, N., and Dascal, N. (2006) Regulation of maximal open probability is a separable function of Ca(v)beta subunit in L-type Ca2+ channel, dependent on NH2 terminus of alpha1C (Ca(v)-1.2alpha. *J. Gen. Physiol. 128*, 15−36.
(30) Altier, C., Garcia-Caballero, A., Simms, B., You, H., Chen, L., Walcher, J., Tedford, H. W., Hermosilla, T., and Zamponi, G. W. (2011) The Cavbeta subunit prevents RFP2-mediated ubiquitination and proteasomal degradation of L-type channels. *Nat. Neurosci. 14*, 173−180.
(31) He, L. L., Zhang, Y., Chen, Y. H., Yamada, Y., and Yang, J. (2007) Functional modularity of the beta-subunit of voltage-gated Ca2+ channels. *Biophys. J. 93*, 834−845.
(32) Berrou, L., Bernatchez, G., and Parent, L. (2001) Molecular determinants of inactivation within the I-II linker of alpha1E (CaV2.3) calcium channels. *Biophys. J. 80*, 215−228.
(33) Berrou, L., Dodier, Y., Raybaud, A., Tousignant, A., Dafi, O., Pelletier, J. N., and Parent, L. (2005) The C-terminal residues in the alpha-interacting domain (AID) helix anchor CaV beta subunit interaction and modulation of CaV2.3 channels. *J. Biol. Chem. 280*, 494−505.
(34) Perez-Reyes, E., Castellano, A., Kim, H. S., Bertrand, P., Baggstrom, E., Lacerda, A. E., Wei, X. Y., and Birnbaumer, L. (1992) Cloning and expression of a cardiac/brain beta subunit of the L-type calcium channel. *J. Biol. Chem. 267*, 1792−1797.
(35) Yamaguchi, H., Okuda, M., Mikala, G., Fukasawa, K., and Varadi, G. (2000) Cloning of the beta(2a) subunit of the voltage-dependent calcium channel from human heart: cooperative effect of alpha(2)/delta and beta(2a) on the membrane expression of the alpha(1C) subunit. *Biochem. Biophys. Res. Commun. 267*, 156−163.
(36) Neely, A., Wei, X., Olcese, R., Birnbaumer, L., and Stefani, E. (1993) Potentiation by the beta subunit of the ratio of the ionic current to the charge movement in the cardiac calcium channel. *Science 262*, 575−578.
(37) Takahashi, S. X., Miriyala, J., Tay, L. H., Yue, D. T., and Colecraft, H. M. (2005) A CaV{beta} SH3/Guanylate Kinase Domain Interaction Regulates Multiple Properties of Voltage-gated Ca2+ Channels. *J. Gen. Physiol. 126*, 365−377.
(38) De Waard, M., and Campbell, K. P. (1995) Subunit regulation of the neuronal alpha 1A Ca2+ channel expressed in Xenopus oocytes. *J. Physiol. 485*, 619−634.
(39) Colecraft, H. M., Alseikhan, B., Takahashi, S. X., Chaudhuri, D., Mittman, S., Yegnasubramanian, V., Alvania, R. S., Johns, D. C., Marban, E., and Yue, D. T. (2002) Novel functional properties of Ca(2+) channel beta subunits revealed by their expression in adult rat heart cells. *J. Physiol. 541*, 435−452.
(40) Bell, D. C., Butcher, A. J., Berrow, N. S., Page, K. M., Brust, P. F., Nesterova, A., Stauderman, K. A., Seabrook, G. R., Nurnberg, B., and Dolphin, A. C. (2001) Biophysical properties, pharmacology, and modulation of human, neuronal L-type (alpha(1D), Ca(V)1.3) voltage-dependent calcium currents. *J. Neurophysiol. 85*, 816−827.
(41) Canti, C., Davies, A., Berrow, N. S., Butcher, A. J., Page, K. M., and Dolphin, A. C. (2001) Evidence for two concentration-dependent processes for beta-subunit effects on alpha1B calcium channels. *Biophys. J. 81*, 1439−1451.
(42) Geib, S., Sandoz, G., Cornet, V., Mabrouk, K., Fund-Saunier, O., Bichet, D., Villaz, M., Hoshi, T., Sabatier, J. M., and De Waard, M. (2002) The interaction between the I-II loop and the III-IV loop of Cav2.1 contributes to voltage-dependent inactivation in a beta -dependent manner. *J. Biol. Chem. 277*, 10003−10013.
(43) Opatowsky, Y., Chomsky-Hecht, O., Kang, M. G., Campbell, K. P., and Hirsch, J. A. (2003) The voltage-dependent calcium channel beta subunit contains two stable interacting domains. *J. Biol. Chem. 278*, 52323−52332.
(44) Butcher, A. J., Leroy, J., Richards, M. W., Pratt, W. S., and Dolphin, A. C. (2006) The importance of occupancy rather than affinity of CaV{beta} subunits for the calcium channel I-II linker in relation to calcium channel function. *J. Physiol. 574*, 387−398.

DOI: 10.1021/acschemneuro.6b00454
ACS Chem. Neurosci. 2017, 8, 1313−1326

(45) Van Petegem, F., Duderstadt, K. E., Clark, K. A., Wang, M., and Minor, D. L., Jr. (2008) Alanine-Scanning Mutagenesis Defines a Conserved Energetic Hotspot in the Ca(V)alpha(1) AID-Ca(V)beta Interaction Site that Is Critical for Channel Modulation. *Structure 16*, 280−294.
(46) Chen, Y. H., Li, M. H., Zhang, Y., He, L. L., Yamada, Y., Fitzmaurice, A., Shen, Y., Zhang, H., Tong, L., and Yang, J. (2004) Structural basis of the alpha1-beta subunit interaction of voltage-gated Ca2+ channels. *Nature 429*, 675−680.
(47) Opatowsky, Y., Chen, C. C., Campbell, K. P., and Hirsch, J. A. (2004) Structural Analysis of the Voltage-Dependent Calcium Channel beta Subunit Functional Core and Its Complex with the alpha1 Interaction Domain. *Neuron 42*, 387−399.
(48) Van Petegem, F., Clark, K. A., Chatelain, F. C., and Minor, D. L., Jr. (2004) Structure of a complex between a voltage-gated calcium channel beta-subunit and an alpha-subunit domain. *Nature 429*, 671−675.
(49) Almagor, L., Chomsky-Hecht, O., Ben-Mocha, A., Hendin-Barak, D., Dascal, N., and Hirsch, J. A. (2012) The role of a voltage-dependent Ca2+ channel intracellular linker: a structure-function analysis. *J. Neurosci. 32*, 7602−7613.
(50) Catterall, W. A., and Swanson, T. M. (2015) Structural Basis for Pharmacology of Voltage-Gated Sodium and Calcium Channels. *Mol. Pharmacol. 88*, 141−150.
(51) Zamponi, G. W. (2016) Targeting voltage-gated calcium channels in neurological and psychiatric diseases. *Nat. Rev. Drug Discovery 15*, 19−34.
(52) Kalia, J., Milescu, M., Salvatierra, J., Wagner, J., Klint, J. K., King, G. F., Olivera, B. M., and Bosmans, F. (2014) From foe to friend: Using animal toxins to investigate ion channel function. *J. Mol. Biol. 427*, 158.
(53) Young, K., Lin, S., Sun, L., Lee, E., Modi, M., Hellings, S., Husbands, M., Ozenberger, B., and Franco, R. (1998) Identification of a calcium channel modulator using a high throughput yeast two-hybrid screen. *Nat. Biotechnol. 16*, 946−950.
(54) Jangsangthong, W., Kuzmenkina, E., Bohnke, A. K., and Herzig, S. (2011) Single-channel monitoring of reversible L-type Ca(2+) channel Ca(V)alpha(1)-Ca(V)beta subunit interaction. *Biophys. J. 101*, 2661−2670.
(55) Hohaus, A., Poteser, M., Romanin, C., Klugbauer, N., Hofmann, F., Morano, I., Haase, H., and Groschner, K. (2000) Modulation of the smooth-muscle L-type Ca2+ channel alpha1 subunit (alpha1C-b) by the beta2a subunit: a peptide which inhibits binding of beta to the I-II linker of alpha1 induces functional uncoupling. *Biochem. J. 348*, 657−665.
(56) Campiglio, M., Di Biase, V., Tuluc, P., and Flucher, B. E. (2013) Stable incorporation versus dynamic exchange of beta subunits in a native Ca2+ channel complex. *J. Cell Sci. 126*, 2092−2101.
(57) Hidalgo, P., Gonzalez-Gutierrez, G., Garcia-Olivares, J., and Neely, A. (2006) The alpha1-beta-subunit interaction that modulates calcium channel activity is reversible and requires a competent alpha-interaction domain. *J. Biol. Chem. 281*, 24104−24110.
(58) Verdine, G. L., and Hilinski, G. J. (2012) Stapled peptides for intracellular drug targets. *Methods Enzymol. 503*, 3−33.
(59) Jo, H., Meinhardt, N., Wu, Y., Kulkarni, S., Hu, X., Low, K. E., Davies, P. L., DeGrado, W. F., and Greenbaum, D. C. (2012) Development of alpha-helical calpain probes by mimicking a natural protein-protein interaction. *J. Am. Chem. Soc. 134*, 17704−17713.
(60) Diderich, P., Bertoldo, D., Dessen, P., Khan, M. M., Pizzitola, I., Held, W., Huelsken, J., and Heinis, C. (2016) Phage Selection of Chemically Stabilized alpha-Helical Peptide Ligands. *ACS Chem. Biol. 11*, 1422−1427.
(61) Aurora, R., and Rosee, G. D. (1998) Helix capping. *Protein Sci. 7*, 21−38.
(62) Mahon, A. B., and Arora, P. S. (2012) End-Capped alpha-Helices as Modulators of Protein Function. *Drug Discovery Today: Technol. 9*, e57−e62.
(63) Timmerman, P., Beld, J., Puijk, W. C., and Meloen, R. H. (2005) Rapid and quantitative cyclization of multiple peptide loops onto synthetic scaffolds for structural mimicry of protein surfaces. *ChemBioChem 6*, 821−824.
(64) Findeisen, F., and Minor, D. L., Jr. (2009) Disruption of the IS6-AID Linker Affects Voltage-gated Calcium Channel Inactivation and Facilitation. *J. Gen. Physiol. 133*, 327−343.
(65) Arias, J. M., Murbartian, J., Vitko, I., Lee, J. H., and Perez-Reyes, E. (2005) Transfer of beta subunit regulation from high to low voltage-gated Ca2+ channels. *FEBS Lett. 579*, 3907−3912.
(66) Berova, N., Nakanishi, K., and Woody, R. W. (2000) *Circular Dichroism: Principles and Applications*, 2nd ed., Wiley-VCH, New York.
(67) Chodera, J. D., and Mobley, D. L. (2013) Entropy-enthalpy compensation: role and ramifications in biomolecular ligand recognition and design. *Annu. Rev. Biophys. 42*, 121−142.
(68) Scholtz, J. M., Marqusee, S., Baldwin, R. L., York, E. J., Stewart, J. M., Santoro, M., and Bolen, D. W. (1991) Calorimetric determination of the enthalpy change for the alpha-helix to coil transition of an alanine peptide in water. *Proc. Natl. Acad. Sci. U. S. A. 88*, 2854−2858.
(69) Zhang, Y., Chen, Y. H., Bangaru, S. D., He, L., Abele, K., Tanabe, S., Kozasa, T., and Yang, J. (2008) Origin of the voltage dependence of G-protein regulation of P/Q-type Ca2+ channels. *J. Neurosci. 28*, 14176−14188.
(70) Findeisen, F., Rumpf, C. H., and Minor, D. L., Jr. (2013) Apo states of calmodulin and CaBP1 control CaV1 voltage-gated calcium channel function through direct competition for the IQ domain. *J. Mol. Biol. 425*, 3217−3234.
(71) Stotz, S. C., Jarvis, S. E., and Zamponi, G. W. (2004) Functional roles of cytoplasmic loops and pore lining transmembrane helices in the voltage-dependent inactivation of HVA calcium channels. *J. Physiol. 554*, 263−273.
(72) Cens, T., Rousset, M., Leyris, J. P., Fesquet, P., and Charnet, P. (2006) Voltage- and calcium-dependent inactivation in high voltage-gated Ca(2+) channels. *Prog. Biophys. Mol. Biol. 90*, 104−117.
(73) Halling, D. B., Aracena-Parks, P., and Hamilton, S. L. (2005) Regulation of voltage-gated Ca2+ channels by calmodulin. *Sci. Signaling 2005*, re15.
(74) Chien, A. J., Gao, T., Perez-Reyes, E., and Hosey, M. M. (1998) Membrane targeting of L-type calcium channels. Role of palmitoylation in the subcellular localization of the beta2a subunit. *J. Biol. Chem. 273*, 23590−23597.
(75) Jencks, W. P. (1981) On the attribution of additivity of binding energies. *Proc. Natl. Acad. Sci. U. S. A. 78*, 4046−4050.
(76) Trimmer, J. S. (1998) Regulation of ion channel expression by cytoplasmic subunits. *Curr. Opin. Neurobiol. 8*, 370−374.
(77) Long, S. B., Campbell, E. B., and Mackinnon, R. (2005) Crystal structure of a mammalian voltage-dependent Shaker family K+ channel. *Science 309*, 897−903.
(78) Pioletti, M., Findeisen, F., Hura, G. L., and Minor, D. L., Jr. (2006) Three-dimensional structure of the KChIP1-Kv4.3 T1 complex reveals a cross-shaped octamer. *Nat. Struct. Mol. Biol. 13*, 987−995.
(79) Ahern, C. A., Payandeh, J., Bosmans, F., and Chanda, B. (2016) The hitchhiker's guide to the voltage-gated sodium channel galaxy. *J. Gen. Physiol. 147*, 1−24.
(80) Bowlby, M. R., Chanda, P., Edris, W., Hinson, J., Jow, F., Katz, A. H., Kennedy, J., Krishnamurthy, G., Pitts, K., Ryan, K., Zhang, H., and Greenblatt, L. (2005) Identification and characterization of small molecule modulators of KChIP/Kv4 function. *Bioorg. Med. Chem. 13*, 6112−6119.
(81) Austin, R. E., Maplestone, R. A., Sefler, A. M., Liu, K., Hruzewicz, W. N., Liu, C. W., Cho, H. S., Wemmer, D. E., and Bartlett, P. A. (1997) Template for stabilization of a peptide alpha-helix: Synthesis and evaluation of conformational effects by circular dichroism and NMR. *J. Am. Chem. Soc. 119*, 6461−6472.
(82) Wang, D., Chen, K., Dimartino, G., and Arora, P. S. (2006) Nucleation and stability of hydrogen-bond surrogate-based alpha-helices. *Org. Biomol. Chem. 4*, 4074−4081.
(83) Yang, S. N., Shi, Y., Yang, G., Li, Y., Yu, J., and Berggren, P. O. (2014) Ionic mechanisms in pancreatic beta cell signaling. *Cell. Mol. Life Sci. 71*, 4149−4177.

DOI: 10.1021/acschemneuro.6b00454
ACS Chem. Neurosci. 2017, 8, 1313−1326

(84) Black, J. A., and Waxman, S. G. (2013) Noncanonical roles of voltage-gated sodium channels. *Neuron 80*, 280−291.
(85) Wulff, H., Castle, N. A., and Pardo, L. A. (2009) Voltage-gated potassium channels as therapeutic targets. *Nat. Rev. Drug Discovery 8*, 982−1001.
(86) Pardo, L. A., and Stuhmer, W. (2014) The roles of K(+) channels in cancer. *Nat. Rev. Cancer 14*, 39−48.
(87) Etemad, S., Obermair, G. J., Bindreither, D., Benedetti, A., Stanika, R., Di Biase, V., Burtscher, V., Koschak, A., Kofler, R., Geley, S., Wille, A., Lusser, A., Flockerzi, V., and Flucher, B. E. (2014) Differential neuronal targeting of a new and two known calcium channel beta4 subunit splice variants correlates with their regulation of gene expression. *J. Neurosci. 34*, 1446−1461.
(88) Tadmouri, A., Kiyonaka, S., Barbado, M., Rousset, M., Fablet, K., Sawamura, S., Bahembera, E., Pernet-Gallay, K., Arnoult, C., Miki, T., Sadoul, K., Gory-Faure, S., Lambrecht, C., Lesage, F., Akiyama, S., Khochbin, S., Baulande, S., Janssens, V., Andrieux, A., Dolmetsch, R., Ronjat, M., Mori, Y., and De Waard, M. (2012) Cacnb4 directly couples electrical activity to gene expression, a process defective in juvenile epilepsy. *EMBO J. 31*, 3730−3744.
(89) Isacoff, E. Y., Jan, L. Y., and Minor, D. L., Jr. (2013) Conduits of life's spark: a perspective on ion channel research since the birth of neuron. *Neuron 80*, 658−674.
(90) Minor, D. L., Jr. (2009) Searching for interesting channels: pairing selection and molecular evolution methods to study ion channel structure and function. *Mol. BioSyst. 5*, 802−810.
(91) Edelhoch, H. (1967) Spectroscopic determination of tryptophan and tyrosine in proteins. *Biochemistry 6*, 1948−1954.
(92) Leslie, A. G. W. (1992) Recent changes to the MOSFLM package for processing film and image plate data, *Joint CCP4 + ESF-EAMCB Newsletter of Protein Crystallography* No. 26, http://www.ccp4.ac.uk/newsletters/No26.pdf.
(93) Evans, P. R. (2011) An introduction to data reduction: space-group determination, scaling and intensity statistics. *Acta Crystallogr., Sect. D: Biol. Crystallogr. 67*, 282−292.
(94) McCoy, A. J., Grosse-Kunstleve, R. W., Adams, P. D., Winn, M. D., Storoni, L. C., and Read, R. J. (2007) Phaser crystallographic software. *J. Appl. Crystallogr. 40*, 658−674.
(95) Emsley, P., and Cowtan, K. (2004) Coot: model-building tools for molecular graphics. *Acta Crystallogr., Sect. D: Biol. Crystallogr. 60*, 2126−2132.
(96) Collaborative Computational Project, No 4. (1994) The CCP4 suite: Programs for protein crystallography. *Acta Crystallogr., Sect. D: Biol. Crystallogr. 50*, 760−763.

DOI: 10.1021/acschemneuro.6b00454
ACS Chem. Neurosci. 2017, 8, 1313−1326